Int. J. Electrochem. Sci., 14 **(2019)** 8048 – 8057, doi: 10.20964/2019.08.78

International Journal of
ELECTROCHEMICAL
SCIENCE
www.electrochemsci.org

Effects of Citric Acid on the Preparation of a $LiFePO_4$@C Cathode Material Assisted by Biomineralization

Linjing Chen[1,2], *Wangjun Feng*[1,2,*], *Zhongsheng Pu*[1,2], *Xuan Wang*[2], *Wenxiao Su*[2], *Miaomiao Li*[2], *Changkun Song*[2], *Zhaojiao Shi*[2], *Yifan Zheng*[2]

[1] State Key Laboratory of Advanced Processing and Recycling Nonferrous Metals, Lanzhou University of Technology, Lanzhou 730050, China
[2] School of Science, Lanzhou University of Technology, Lanzhou 730050, China
[*]E-mail: wjfeng@lut.cn

Received: 6 April 2019 / *Accepted:* 29 May 2019 / *Published:* 30 June 2019

A carbon-coated $LiFePO_4$ (LFP@C) cathode material was prepared by a bio-template-assisted sol-gel method in which yeast acts both as a structural template and as a carbon source. Citric acid monohydrate as a chelating agent was added in different experimental steps to investigate its effect on the crystallinity, specific capacity and electrochemical performance of the positive electrode material LFP. Systematic studies show that LFP@C-3 exhibits the best specific capacity, with discharge capacities of 156.4 mAh g^{-1} and 97.5 mAh g^{-1} at 0.1 C and 5 C, respectively. The improved electrochemical properties of the resulting LFP@C-3 can be attributed to its good crystal purity and carbon coating. The chelating agent citric acid has important positive significance when preparing LFP@C by the sol-gel method and using yeast as a structural template.

Keywords: LFP@C, yeast, sol-gel method, chelating agent, structural template.

1. INTRODUCTION

The growing energy crisis and severe environmental pollution are issues that humanity must face in the 21st century [1]. To alleviate the energy crisis and make more effective use of existing energy sources, researchers have made great efforts in the fields of energy photocatalysis and storage [2,3]. Developing environmentally friendly, sustainable and reusable energy supplies is critical to meeting the energy needs of modern societies. Excellent reversible energy storage equipment has attracted widespread attention [4]. Olivine-structured lithium iron phosphate ($LiFePO_4$) is considered to be the most promising cathode material for lithium-ion batteries (LIBs), and its inherent advantages are environmental friendliness, a high safety factor, low price, and non-toxicity [5]. Unfortunately, the low electronic conductivity (10^{-9}-10^{-10} S cm^{-1}) [6,7] and poor lithium ion diffusivity (10^{-14} cm^2 S^{-1}) [4]

limit the use of $LiFePO_4$ (LFP) in LIBs. To overcome these obstacles, progressive efforts, including alien ion doping [8–10], particle size minimization [11,12] and carbon coating [13,14], have been devoted to improving the electrochemical performance of LFP. Coating a carbon layer on the surface of the cathode material can not only improve the conductivity of the positive electrode material but also effectively control the particle size of the material [15].

Graphene and carbon nanotubes have achieved good results as a carbon source coated on LFP in terms of improving electrochemical performance [4,16], but such materials are difficult to commercialize due to the complicated preparation process and high price. Biological systems can provide unusual structures as an activated carbon [17,18]. Biomineralization refers to the process by which organisms produce inorganic minerals through the regulation of biological macromolecules [19]. Yeast cells can use self-assembly to control the mineralization of nanomaterials. Baker's yeast, having an elliptical morphology, is a single-cell eukaryotic microorganism. Yeast has the advantages of a wide range of sources, low price, easy cultivation and no environmental pollution. More importantly, yeast has abundant surface charge, which is extremely beneficial for biomineralization. Mesoporous bio-carbon-coated $Li_3V_2(PO_4)_3$ has been synthesized, using waste brewing yeast as a bio-carbon source [20]. This excellent nanostructure facilitates electron and lithium ion diffusion.

LFP can be synthesized by hydro- and salvo-thermal synthesis methods [21,22], solid state reactions [23] or sol-gel methods [24,25]. As an advanced method for preparing nanoparticles, the sol-gel method can form a uniform precursor at the molecular level. In this experiment, citric acid was used as a chelating agent in the sol-gel method to synthesize LFP. One of the benefits of citric acid is that it does not pollute the environment because it is a natural substance. Citric acid combines very easily with minerals and metals, which is called chelation. Citric acid has a pair of lone electrons in the hydroxyl group, which can form a stable mixture with the vacant orbital of metal ions [26]. Furthermore, yeast was used as a biological template for the preparation of LFP@C due to its unique morphology and remarkable biomineralization properties.

Here, we use the combination of the sol-gel method and biomineralization to prepare LFP@C. The aim is to find that citric acid as a chelating agent can promote the biomineralization ability of yeast. LFP@C maintains the spherical morphology of the yeast, which means that the yeast acts as a template.

2. EXPERIMENTAL

2.1 Material preparation

In the typical route, $LiOH{\cdot}H_2O$, $FeCl_2{\cdot}4H_2O$ and $NH_4H_2PO_4$ were used as precursors in a molar ratio of 1:1:1. The amount of citric acid ($C_6H_8O_7{\cdot}H_2O$) used here as a chelating agent was the sum of the total amount of metal cations. Instant dry yeast (20 g) was cultivated in a solution of glucose for 1 h at 35 ℃. After magnetic stirring for 1 h, the yeast cell suspension was centrifuged and washed several times with distilled water to obtain purified yeast cells. $FeCl_2{\cdot}4H_2O$ was dissolved in deionized water, and the purified yeast cell solution was added with magnetic stirring for 4 h to obtain

a Fe-yeast cell mixture solution. For the synthesis of the first LFP@C, namely, LFP@C-1, $NH_4H_2PO_4$ and $LiOH·H_2O$ were slowly introduced into the Fe-yeast cell mixture solution in sequence. Finally, citric acid was added to the mixture. For the synthesis of the second LFP@C, namely, LFP@C-2, $NH_4H_2PO_4$ was slowly introduced into the Fe-yeast cell mixture solution followed by the addition of citric acid. Finally, $LiOH·H_2O$ was added to the mixture. For the synthesis of the third LFP@C, namely, LFP@C-3, an aqueous solution of citric acid monohydrate was slowly introduced into the Fe-yeast cell mixture solution, followed by the addition of $NH_4H_2PO_4$. Finally, $LiOH·H_2O$ was added to the mixture. All the above experiment steps were carried out at room temperature. The following experimental steps were the same for all materials: After magnetic stirring for half an hour, the solution was placed in a water bath at 80 ℃ until a gel was formed. The resulting gel was then dried in an oven for 12 h at a temperature of 140 ℃. The precursor was pre-sintered at 350 ℃ for 4 h under an argon atmosphere and then further annealed at 800 ℃ for 10 h.

2.2 Material characterization

To observe the structures of the prepared samples, X-ray diffraction (XRD) was performed using a Bruker D8 Advance diffractometer. XRD patterns were collected in a 2 θ range of 10° - 80°. Transmission electron microscopy (TEM) and high-resolution transmission electron microscopy (HRTEM) at 200 kV were carried out on a JEOL instrument to characterize the interior morphologies of the cathode materials.

2.3 Electrochemical measurements

Electrochemical measurements were performed with CR2025 coin cells. The cathode materials were prepared by mixing dried $LiFePO_4$ (80 wt%), acetylene black (10 wt%) and polyvinylidene fluoride (PVDF, 10 wt%) and, blending in *N*-methylpyrrolidone. The resulting slurry was cast on Al-foil and dried at 120 ℃ for 12 h in a vacuum oven. During the assembly of the CR2025 coin-type cells, Celgard 2400 was used as the separator, and metal lithium was used as the anode. The charge-discharge cycling performances were determined on a Land-CT2001A testing instrument between 2.4 V and 4.2 V versus Li/Li^+ at 0.1 C, 0.5 C, 2 C and 5 C rates (1 C = 170 mAh g^{-1}). Cyclic voltammetry (CV) tests were performed on a CHI 660E electrochemical work station at a scan rate of 0.1 mV s^{-1}. Electrochemical impedance spectroscopy (EIS) tests were carried out at the same electrochemical work station over a frequency ranging from 0.1 Hz to 100 kHz.

3. RESULTS AND DISCUSSION

3.1. Crystalline structure analysis

Fig. 1 shows the X-ray diffraction (XRD) patterns of the as-made samples. As shown in Fig. 1, all diffraction peaks of LFP@C-3 are quite narrow and symmetric, indicating the good crystalline

structure corresponding to orthorhombic-structured LFP (JCPDS # 83-2092, a=10.334 Å, b=6.010 Å, c=4.693 Å) [4] without any impurity phase observed. The absolute lattice parameters (a = 10.32966 Å, b = 6.00709 Å, c = 4.68884 Å) are close to the standard values. No obvious peaks of bio-carbon were detected, implying that citric acid and yeast cells decompose into amorphous carbon. However, from the XRD patterns of the as-obtained LFP@C samples, extra diffraction lines are observed on LFP@C-1 and LFP@C-2, which are attributed to undesired impurities. These impurities are $Li_2Fe_3O_4$ (JCPDS # 037-1432) and $FePO_4$ (JCPDS # 003-0379). Although the peaks are very weak, it is considered that the two samples are of poorer quality. Fe^{2+} binds to the negative ion groups of yeast during yeast biomineralization. Citric acid causes rapid precipitation of metal ions, which may be beneficial to the synthesis of LFP. Chelating agents facilitate the formation of a uniform gel that facilitates the mixing of metal cations at the molecular level during the gel process. Citric acid binds to metal ions to form a uniform precursor gel with a preferred particle size through a carboxyl or hydroxyl group. Comparing the prepared cathode materials, it was found that the crystallinity of LFP was improved by the citric acid-assisted biomineralization process.

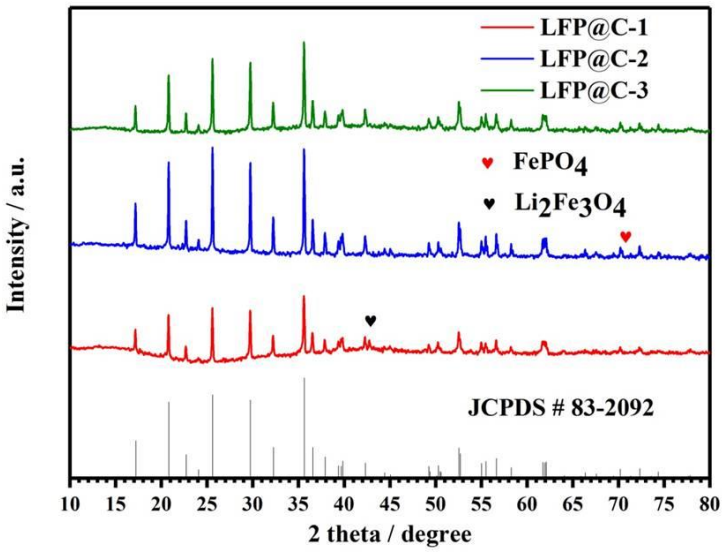

Figure 1. XRD spectra of LFP@C samples prepared with different experimental protocols.

3.2 Morphological observation

Fig. 2 shows the TEM and HRTEM images of the LFP@C-3 sample. In Fig. 2 (a) and (b), particles with elliptical morphology are observed, indicating that the yeast cells act to regulate the morphology because the appearance is similar to yeast cell morphology. In addition, the sample consists of two parts, LFP and a carbon net. There are two sources of carbon networks: one is obtained by the thermal decomposition of the chelating agent citric acid, and the other is obtained by the carbonization of yeast cells. To further explore this perfect nanostructure, HRTEM analysis was performed. As shown in Fig. 2 (c), the structure of the sample is a composite of the nanocomposite structure and bio-carbon network structure. The bio-carbon network surrounds the nanoparticle, and the nanoparticle is located at the centre. The carbon network helps to improve the electronic

conductivity and promote electrolyte penetration. The thickness of the bio-carbon layer coated on the surface of the particles is approximately 5-8 nm. During calcination, yeast and citric acid are decomposed and carbonized in an inert atmosphere. To improve conductivity and facilitate lithium ion penetration, it is necessary to select an appropriate carbon coating thickness. The material delivers the largest specific discharge capacity when the surface of the LFP is coated with a carbon layer with a thickness of 4-8 nm [27-30]. Fig. 2 (d) clearly reveals that the interlayer spacing is 0.392 nm, which corresponds to the (210) plane of LFP crystals.

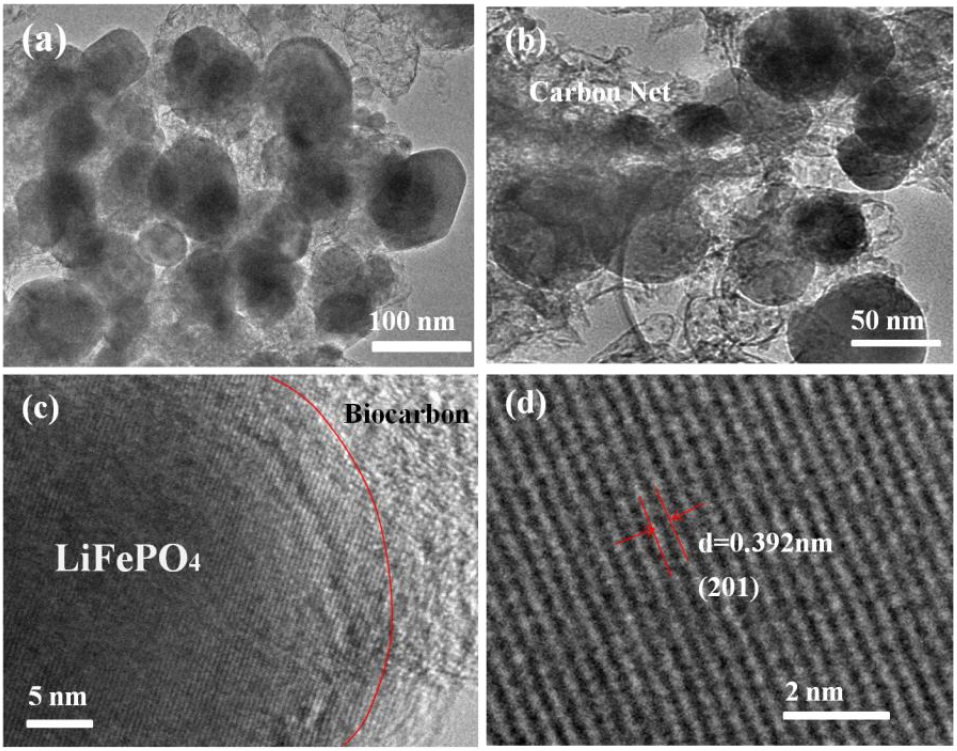

Figure 2. (a), (b) TEM micrographs and (c), (d) HRTEM images of LFP@C-3.

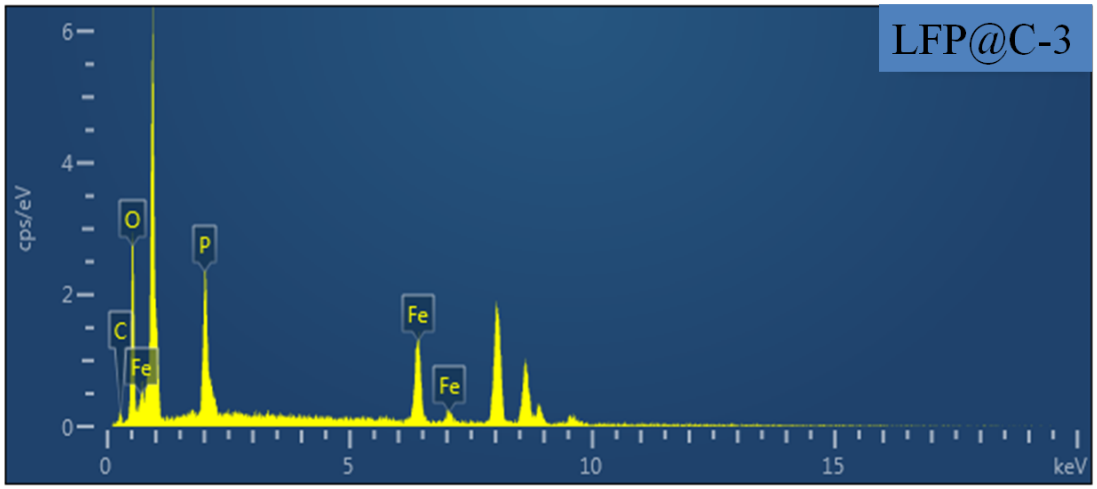

Figure 3. EDS spectrum of LFP@C-3

Table 1. Content of each element in the LFP@C-3 sample

element	wt%	wt% Sigma	Atomic %
C	6.94	2.60	13.55
O	40.63	1.58	59.52
P	14.64	0.77	11.08
Fe	37.79	1.49	15.86
Total amount:	100.00		100.00

The energy-dispersive spectroscopy (EDS) spectrum shown in Fig. 3 further confirms the content of elements in the prepared materials. EDS indicates that LFP@C-3 is composed of C, O, P and Fe and no impurities, which is consistent with the XRD detection results. The carbon content in the prepared sample LFP@C-3 is confirmed to be 6.94 wt% (Table. 1). The conductivity of the LFP@C-3 material is closely related to the conductivity of synthetic carbon materials. Carbon materials are important for improving the electrochemical performance of LFP@C-3.

3.3 Electrochemical performances

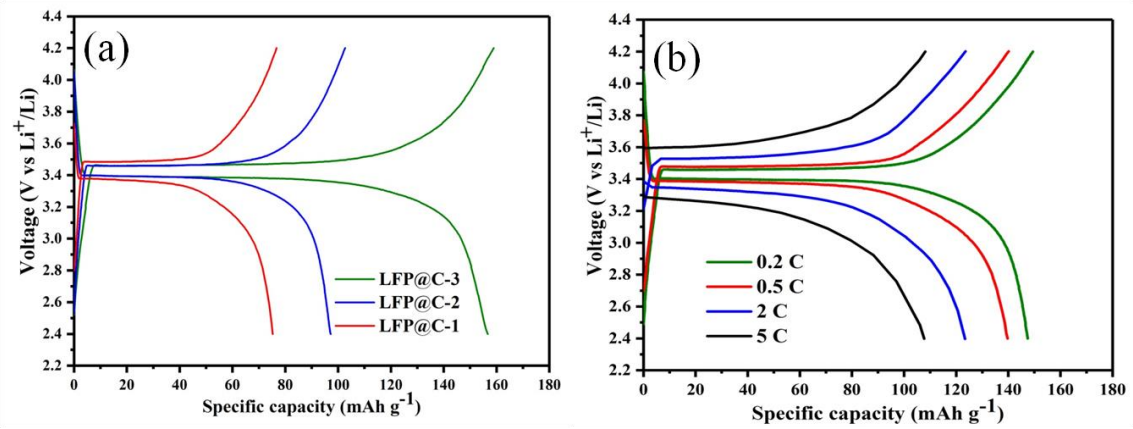

Figure 4. (a) Initial charge-discharge curves of the prepared electrode materials at 0.1 C, (b) Charge-discharge curves of LFP@C-3 at different rates of 0.2 C, 0.5 C, 2 C and 5 C.

The composite electrode material was assembled in a coin cell battery to test its electrochemical performance in the voltage range of 2.4-4.2 V. It is fully demonstrated that the chelating agent plays a crucial role in the preparation of LFP@C by the bio-assisted sol-gel method. The electrochemical performance of the carbon-coated LFP materials, namely, LFP@C-1, LFP@C-2, LFP@C-3, is shown in Fig. 4 (a). Compared with the other two samples, LFP@C-3 shows the best discharge specific capacity (approximately 157 mAh g^{-1} at 0.1 C). In contrast, for LFP@C-2 and LFP@C-1, the discharge capacities are 97 mAh g^{-1} and 75 mAh g^{-1} at 0.1 C, respectively. The possible cause of this phenomenon is the presence of the impurities $Li_2Fe_3O_4$ and $FePO_4$ in LFP@C-2 and

LFP@C-1. Comparison of these results with LFP materials prepared with spirulina and yeast as bio-templates (Table. 2), shows that the specific capacity of the cathode material prepared by using yeast as a template is higher. This can be attributed to the spherical or elliptical shape of the yeast, which is advantageous for improving conductivity in all directions. In addition, the obvious advantage of sol-gel over hydrothermal methods is that the preparation process is simpler. Based on the above results, the LFP@C-3 cathode material was further investigated with respect to its rate capacities **(**Fig. 4 (b)). When the current density increased to 0.2 C, 0.5 C, 2 C and 5 C rates at room temperature, LFP@C-3 presented high initial discharge capacities of approximately 147 mAh g^{-1}, 140 mAh g^{-1}, 124 mAh g^{-1} and 108 mAh g^{-1}, respectively, which indicates good rate performances. As the C rate increases, the storage capacity of the electrode is reduced, and the polarization of the electrode material may increase, which may lead to an increase in electrode resistance. Higher capacity and lower polarization result in optimized electron transport, which is undoubtedly a great advantage in practical applications [31-34].

Table 2. Comparison of this work to current reports of bio-templates used in the preparation of LFP.

Biological template	Preparation method	Rate performance (0.1 C)	Preparation process	Ref
spirulina	Hydrothermal reaction	139 mAh g^{-1}	complex	[34]
yeast	Hydrothermal reaction	158.6 mAh g^{-1}	complex	[35]
yeast	Sol-gel reaction	157 mAh g^{-1}	simple	This work

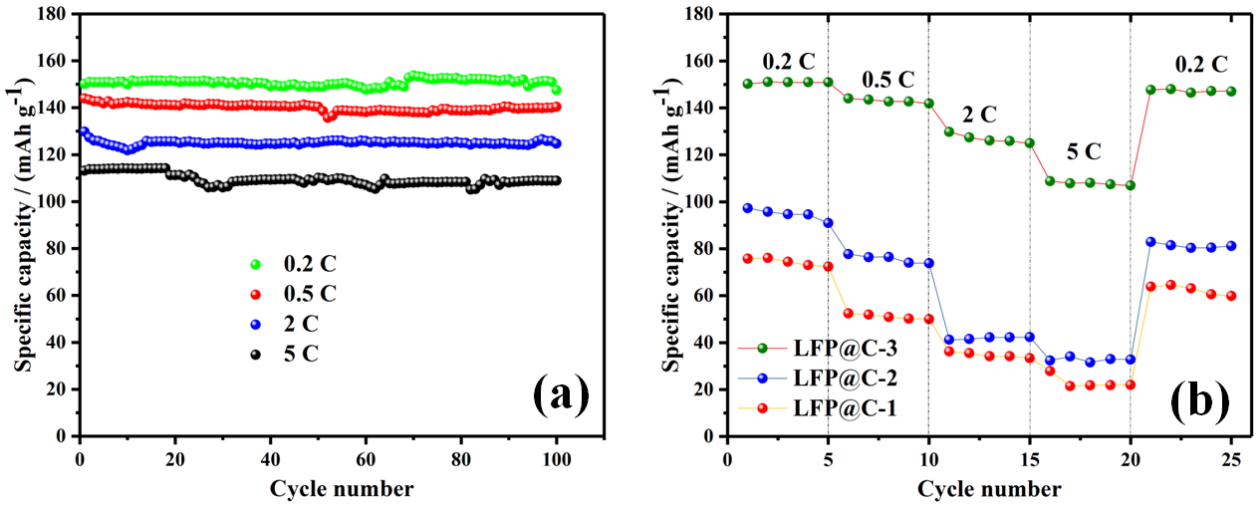

Figure 5. (a) Long-term cycling stabilities at 0.2 C, 0.5 C, 2 C and 5 C of LFP@C-3, (b) Rate capabilities from 0.2 C to 5 C of LFP@C-1, LFP@C-2 and LFP@C-3.

Fig. 5 (a) displays another property of the LFP@C-3, the cycling performance. LFP@C-3 exhibits the best rate performance, with a discharge capacity of approximately 147 mAh g^{-1}, 140 mAh

g^{-1}, 124 mAh g^{-1} and 108 mAh g^{-1} at 0.2 C, 0.5 C, 2 C and 5 C, respectively, in the last recorded cycle. Good cycle stability can be attributed to the high degree of crystallinity of the prepared material without impurities and the formation of a uniform carbon coating on the surface of the positive electrode material. The reason why the specific capacity gradually rises after 20 charge and discharge cycles may be that the lithium ions inside the LFP particles are well extracted/embedded in the charge and discharge process as the number of charge cycles increases at the rate of 0.5 C. The cycling performance in every first 5 cycles at 0.2-5 C rates are displayed in Fig. 5 (b). It can be clearly seen that the specific capacity of LFP@C-3 is much higher than the specific capacities of LFP@C-1 and LFP@C-2 at rates of 0.2 C, 0.5 C, 2 C and 5 C. When recovering the former testing conditions (0.2 C), the discharge capacities decrease by no more than 4 mAh g^{-1}. The LFP@C-3 sample is pure and free of impurities, suggesting an excellent reversible specific capacity.

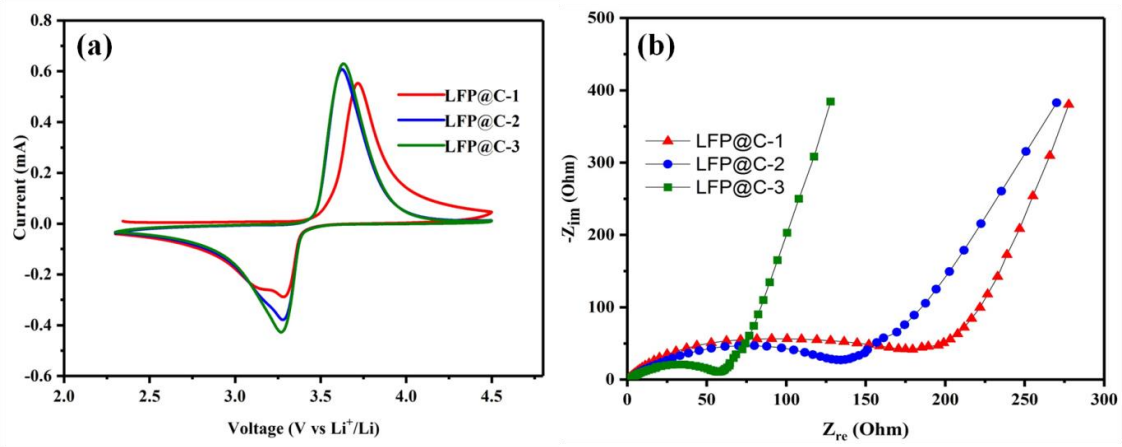

Figure 6. (a) Cyclic voltammetry profiles of LFP@C-1, LFP@C-2 and LFP@C-3 at a scan rate of 0.5 mV s^{-1}, (b) EIS profiles of LFP@C-1, LFP@C-2 and LFP@C-3 before cycling

Cyclic voltammetry (CV) is a useful electrochemical method for determining the reversibility of microscopic reaction processes and electrode reactions on electrode surfaces. Fig. 6 (a) compares the CV curves of the prepared samples measured at a scanning rate of 0.5 mV s^{-1}. The CV curves of the three samples all showed obvious anodic/cathodic peaks, which correspond to the process of lithium ion elution and embedding in the crystal. The oxidation peaks and reduction peaks of LFP@C-1 and LFP@C-2 are asymmetrical, which indicates that the diffusion of lithium ions in these two samples is not smooth. The order of peak current is LFP@C-3 > LFP@C-2 > LFP@C-1, which implies that LFP@C-3 has the best lithium ion diffusivity. The almost equal oxidation peak area and reduction peak area indicate the better reversibility of LFP@C-3. Fig. 6 (b) presents the EIS responses for all of the samples. The graph consists of a suppressed semicircle associated with charge transfer resistance and corresponding capacitance at the electrode/electrolyte interface and a linear Warburg portion associated with diffusion of lithium ions in the electrode body [36]. The LFP@C-3 composite has smaller semicircles than LFP@C-2 and LFP@C-1, indicating a lower resistance to charge transfer

of the LFP@C-3 composite. Furthermore, the impedance slopes of LFP@C-3 in the low-frequency range reflect the enhanced mobility of Li ions in electrode LFP@C-3.

4. CONCLUSIONS

In conclusion, an LFP@C-3 composite with spherical morphology has been prepared by a sol-gel method using yeast as a structural template and citric acid as a chelating agent, added in different experimental steps. LFP@C-3 with a good lattice structure was prepared by simply adjusting the feeding sequence of the chelating agent in the sol-gel process. XRD and TEM demonstrate that LFP@C-3 has perfect crystallinity and a uniform distribution of spherical morphology. Citric acid acts as a chelating agent to inhibit the formation of impurities that favour the formation of perfect LFP crystals. In contrast, LFP@C-3 exhibits the best electrochemical performance. The initial discharge capacity reaches 157 mAh g^{-1} at 0.1 C in the potential range of 2.4-4.2 V. This study demonstrates the positive impacts of both yeast cells and citric acid in terms of providing active sites for nuclei and increasing the electronic conductivity. The method described in this paper is a cost-effective, efficient and environmentally friendly approach, that is worth popularizing.

ACKNOWLEDGEMENTS
This work was financially supported by the National Natural Science Foundation of China (Grant No.11264023) and the HongLiu First-class Disciplines Development Program of Lanzhou University of Technology.

References

1. C. Gong, Z. Xue, S. Wen, Y. Ye and X. Xie, *J. Power Sources.*, 318 (2016) 93.
2. Y. Yan, H. Yang, X. Zhao, R. Li and X. Wang, *Mater. Res. Bull.*,105 (2018) 286.
3. W.X. Su, W.J. Feng, Y. Cao, L.J. Chen, M.M. Li and C.K. Song, *Int. J. Electrochem. Sci.*, 13 (2018) 6005.
4. S. Chen, Q. Tang, X. Chen and L. Tan, *New J. Chem.*, 39 (2015) 9782.
5. Y. Chen, K. Xiang, W. Zhou, Y. Zhu, N. Bai and H. Chen., *J. Alloys Compd.*, 749 (2018) 1063.
6. L. Wang, X. He, W. Sun, J. Wang, Y. Li and S. Fan, *Nano Lett.*, 12 (2012) 5632.
7. L.-L. Zhang, G. Liang, A. Ignatov, M.C. Croft, X.-Q. Xiong, I.-M. Hung, Y.-H. Huang, X.-L. Hu, W.-X. Zhang and Y.-L. Peng, *J. Phys. Chem. C.*, 115 (2011) 13520.
8. Z. Yang, J. Xia, L. Zhi, W. Zhang and B. Pei, *Ionics.*, 20 (2013) 169.
9. X. Zhao, D.-H. Baek, J. Manuel, M.-Y. Heo, R. Yang, J.K. Ha, H.-S. Ryu, H.-J. Ahn, K.-W. Kim, K.-K. Cho and J.-H. Ahn, *Mater. Res. Bull.*, 47 (2012) 2819.
10. S. Yoon, C. Liao, X.-G. Sun, C.A. Bridges, R.R. Unocic, J. Nanda, S. Dai and M.P. Paranthaman, *J. Mater. Chem.*, 22 (2012) 4611.
11. Y. Wang, Z. Liu and S. Zhou, *Electrochimica Acta.*, 58 (2011) 359.
12. Y. Wang, Y. Wang, E. Hosono, K. Wang and H. Zhou, *Angew. Chem.*, 120 (2008) 7571.
13. Y. Wu, Z. Wen and J. Li, *Adv. Mater.*, 23 (2011) 1126.
14. B.L. Ellis, K.T. Lee and L.F. Nazar, *Chem. Mater.*, 22 (2010) 691.
15. G. Lei, X. Yi, L. Wang, Z. Li and J. Zhou, *Polym. Adv. Technol.*, 20 (2009) 576.

16. H. Wu, Q. Liu and S. Guo, *Nano-Micro Lett.*, 6 (2014) 316.
17. W. Wu, J. Pu, J. Wang, Z. Shen, H. Tang, Z. Deng, X. Tao, F. Pan and H. Zhang, *Adv. Energy Mater.*, 8 (2018) 1702373.
18. E. Brunner, C. Gröger, K. Lutz, P. Richthammer, K. Spinde and M. Sumper, *Appl. Microbiol. Biotechnol.*, 84 (2009) 607.
19. J. Han, Y. Dou, D. Yan, J. Ma, M. Wei, D.G. Evans and X. Duan, *Chem. Commun.*, 47 (2011) 5274.
20. W. He, X. Zhang, X. Du, Y. Zhang, Y. Yue, J. Shen and M. Li, *Electrochimica Acta.*, 112 (2013) 295.
21. F. Brochu, A. Guerfi, J. Trottier, M. Kopeć, A. Mauger, H. Groult, C.M. Julien and K. Zaghib, *J. Power Sources.*, 214 (2012) 1.
22. X. Li, D. Luo, X. Zhang and Z. Zhang, *J. Power Sources.*, 291 (2015) 75.
23. Y. Wang, Z.-S. Feng, J.-J. Chen, C. Zhang, *Mater. Lett.*, 71 (2012) 54.
24. J. Yang, J. Wang, X. Li, D. Wang, J. Liu, G. Liang, M. Gauthier, Y. Li, D. Geng, R. Li and X. Sun,, *J. Mater. Chem.*, 22 (2012) 7537.
25. J. Yang, J. Wang, Y. Tang, D. Wang, B. Xiao, X. Li, R. Li, G. Liang, T.-K. Sham and X. Sun, *J. Mater. Chem. A.*, 1 (2013) 7306.
26. G. Xie, H.-J. Zhu, X.-M. Liu and H. Yang, *J. Alloys Compd.*, 574 (2013) 155.
27. Y.-D. Cho, G.T.-K. Fey and H.-M. Kao, *J. Power Sources.*, 189 (2009) 256.
28 J. Wang and X. Sun, *Energy Env. Sci*, 5 (2012) 5163.
29 B. Zhao, Y. Jiang, H. Zhang, H. Tao, M. Zhong and Z. Jiao, *J. Power Sources*, 189 (2009) 462.
30 R. Dominko, M. Bele, M. Gaberscek, M. Remskar, D. Hanzel, S. Pejovnik and J. Jamnik, *J. Electrochem. Soc.*, 152 (2005) A607.
31 K. Saravanan, P. Balaya, M.V. Reddy, B.V.R. Chowdari and J.J. Vittal, *Energy Environ. Sci.*, 3 (2010) 457.
32 J. Zhang, N. Nie, Y. Liu, J. Wang, F. Yu, J. Gu and W. Li, *ACS Appl. Mater. Interfaces.*, 7 (2015) 20134.
33 T. Liu, L. Zhao, J. Zhu, B. Wang, C. Guo and D. Wang, *J Mater Chem A.*, 2 (2014) 2822.
34 Y. Xia, W. Zhang, H. Huang, Y. Gan, Z. Xiao, L. Qian and X. Tao, *J. Mater. Chem.*, 21 (2011) 6498.
35 Y. Cao, W.J. Feng *and* W.X. Su, *Int. J. Electrochem. Sci.*, 13 (2018) 8022.
36 J.Y. Xiang, J.P. Tu, L. Zhang, X.L. Wang, Y. Zhou, Y.Q. Qiao and Y. Lu, *J. Power Sources.*, 195 (2010) 8331.